Dynamic control of polarized thermal emission from VO_2 nanofins

Caleb A. Estherby[a], **Matthew D. Arnold**[a], **Matthew C. Tai**[a], **Angus R. Gentle**[a*]
[a]University of Technology Sydney, Mathematical and Physical Sciences, PO Box 123, Ultimo NSW, 2007, Australia

Abstract. Here we demonstrate switchable polarized thermal emission from VO_2 nano-fin stacks fabricated by co-deposition, etching and oxidation. We find that reverse switching of the thermal emission is enabled by a reflecting underlayer, induced by either short oxidation time or additional deposition of a reflecting underlayer. Observed thermal emission is well explained by a biaxial Bruggeman effective medium model, which predicts the strong polarization change for aligned fin layers in the micron thickness range. The dominant polarization of the emission is modulated by the presence of a reflector, oxidation of the fins, fin fill-factor, and structural anisotropy. Normal incidence polarized emittance change of up to 0.6 is theoretically possible, and we were able demonstrate a change of 0.34 similar to that predicted by the model.

Keywords: vanadium dioxide, polarization, thermal emission, nanostructured.

*Dr. Angus Gentle, angus.gentle@uts.edu.au

1 Introduction

Dynamic control of thermal emission is an area of considerable interest, with application in areas such as thermal regulation, active camouflage, and sensing. A common strategy for varying thermal emission is to use phase change materials (PCM), such as $Ge_2Sb_2Te_5$(GST) or vanadium dioxide (VO_2), which have an associated change in their thermal infrared properties.

GST has been used for optical modulation due to a difference in reflectivity of its amorphous and crystalline phases.[1] GST has also been utilised for control of thermal emission including application in thermal camouflage and as a wavelength-selective and thermally stable IR emitter.[2,3] However, while GST benefits from the stability of the crystalline phase, a consequential drawback is that it must be annealed above 640°C to return it to the amorphous state, which makes it unsuitable for some applications.[4]

In contrast VO_2 has a readily reversible transition near room temperature, and will be our focus in this article. The rapid insulator-metal transition can be activated by thermal, optical and

electrical stimulation.[5,6] Several applications have made use of this functionality,[7–10] in particular modulated emission for thermal regulation.[11]

The usual mechanism of emission control in VO_2 devices is that the bulk switches from high to low emissivity on heating due to the increase in charge carriers, thereby reducing radiated heat.[12] VO_2 is often used as a phase-changing material in or near photonic structures, for example for adaptively enabling radiative cooling, depending on the ambient temperature.[13] Likewise, by using $\sim$150 nm of VO_2 on sapphire Kats et al. were able to display a near "perfect" black body emittance at a single wavelength. This was achieved through the insulator to metal transition (IMT) of VO_2. Interestingly, the intermediary state of the VO_2 consists of nanoscale islands of conducting and insulating phases, acting as a natural, disordered meta-material,[14] which is readily modelled with a Bruggeman effective medium model.[15,16]

Recent attention has focused on inverted emission switching (increasing with heating), allowing abruptly increased radiative cooling and enhanced temperature regulation. Inverted switching has been achieved by structuring including multi-layers,[17,18] lithography,[19,20] and self-assembly.[21] In our recent work, vanadium oxide nano-fins were produced by a lithography-free method consisting of co-deposition with aluminum followed by chemical removal of the aluminum and then gaseous oxidation. Varying fin height achieved a variety of switching profiles, including reverse switching.

A similar method was used in a different paper to produce Mo fins which were shown to be heat-stable polarizers.[22] Therefore it is expected that VO_2 fins (such as those seen in Fig.1), would enable switchable polarized thermal emission near the normal direction, with applications such as infrared instrumentation. So far, comparatively little progress has been made towards this functionality. One relevant work[23] demonstrated a different approach using elliptical metal

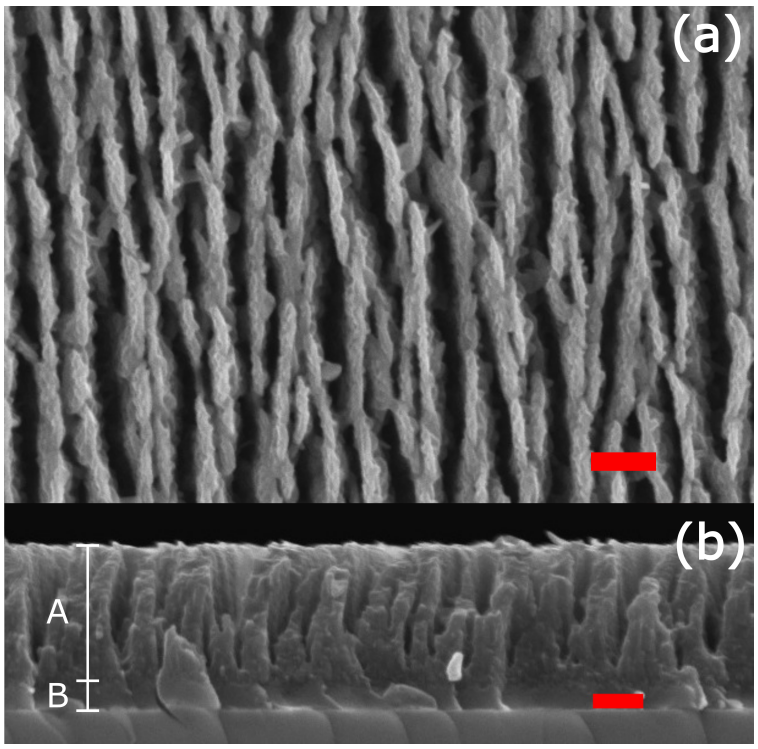

Fig 1 SEM image of a typical nanostructured VO_2 thin film on glass. (a) showing top view and (b) showing the cross-section view. (Scale bar 200nm). The polarization convention used in this article refers to the in-plane fin axes, i.e. perpendicular is left-right in both panels, parallel is top-bottom in (a). In (b) 'A' indicates the fins while 'B' indicates the native reflector.

patches on GST, with simulations predicting up to 0.7 absolute emittance difference and high ratio. However, that design required lithography, and measured performance was only about 0.1 absolute difference and ratio ~ 2. Furthermore, this polarizing surface is unable to function near normal angles.

The approach that we present in this article does not require lithography, achieves high absolute polarization over a comparatively broad spectral range, operates at near normal angles and demonstrates reversible switching at modest temperatures.

We first demonstrate the ability to choose the direction of the switch by controlling the oxidation state, then predict how the switch can be reversed and optimized by simple geometric changes, and finally demonstrate strongly polarized emission.

2 Experimental

We produced VO_2 nano fins using a three-step process:[21] self-assembly of V-Al fins, dissolution of Al using NaOH to form vanadium fins, followed by controlled oxidation during annealing. First V-Al fins were produced by co-sputtering of V and Al. The targets were spaced 150 mm apart from one another with a 37 °angle to the stage normal at the center of the target, with an angular spread (30°-46°) due to target size. The alloy fins were placed into 1 M NaOH for 13 minutes to selectively etch the Al from the alloy, leaving V fins, similar to our previous work.[22] The final step in production was the oxidation of the fins by annealing in sub-atmospheric (0.2 Torr) air. A carbon heating block maintained the films at approximately 500°for several hours to produce the desired VO_2 phase. In some samples, 200 nm of pure vanadium was deposited on the substrate before the nanofin structure was deposited. The switching of thermal emission on heating and cooling from 30 to 80 °C was measured via three techniques: (1) spectrally-integrated unpolarized emission, (2) infrared reflectance and (3) spectrally-resolved polarized emission measurements. Method 1 - The integrated measurements were estimated from the apparent radiant temperature T_{IR} using equation 1. It is important to account for the sample temperature and reflected temperatures to accurately determine the emittance of the surface being tested. Using an infrared sensor that returns a temperature measured in Kelvin we can use Equation 1 to determine the emittance of the sample E and temperature.[21]

$$\epsilon(T) = \frac{T_{IR}^4 - T_{Reflected}^4}{T_{Sample}^4 - T_{Reflected}^4} \tag{1}$$

This method provides a fast technique to assess a sample's temperature-dependent emittance performance, for example in Fig 3, prior to detailed temperature-dependent spectral measurements of

a sample.

$$\epsilon(T) = \frac{\int A(\lambda) * B(\lambda, T) d\lambda}{\int B(\lambda, T) d\lambda} \tag{2}$$

Likewise once the spectral properties of a surface are known we can use Equation 2 to calculate the temperature dependent emittance. E(T) is the integrated emittance, A(λ) is the absorption properties of the surface and B(λ, T) is the black body Planck spectrum for each wavelength(λ) and temperature(T). In the case of temperature dependent optical properties A(λ,T) can be substituted in for A(λ). Equation 2 can be used to compare results measured via Method 2 and Method 1.

Method 2 - FTIR (Fourier Transform Infrared) reflection spectroscopy was performed with a Perkin-Elmer Spectrum 100 FT-IR Spectrometer with a Harrick SeaGull variable-angle reflection stage (modified with a sample heating stage) and infrared wire-grid polarizer in a 2.5-25 μm wavelength range, with incidence angles varying from 10 to 45°. Samples were measured at 25°C and 90°C (cold and hot states). These reflection measurements were performed on both solid and structured films, and were used to establish model parameters and to validate direct emission measurements.

The ellipsometric software WVASE, by JA Woollam Co, was used to fit the complex refractive index of each of the solid thin film samples (VO_2 in both the cold "semiconducting" and hot "metallic" states, thin film sputtered vanadium and glass substrates), with generalized oscillator models produced for each material.

The nano-fin structure was modelled by a biaxial Bruggeman effective-medium layer with geometric depolarization factors for in-plane and stack directions.[24] This is a well-established model that we have successfully applied to similar structures in earlier work. Bulk VO_2 properties for hot and cold states were based on fits to solid thin films. To ensure consistency of geometric

parameters, fitting of the fill factor and depolarization factors in the biaxial Bruggeman model was simultaneously conducted in both the low and high temperature states with parameters linked.

The intermediate temperature response of the bulk VO_2 was incorporated using a Bruggeman[25] effective medium model, as suggested in.[15,16] A sigmoidal model was used to fit $f(T)$ the fraction of solid material which has undergone the transition into the metallic state for each temperature. This was supported by additional temperature dependent ellipsometry from 0.3 - 3 microns (Woollam V-VASE with custom temperature stage).

$$f(T) = \frac{e^{(T-T_c)*P_1}}{e^{(T-T_c)*P_1} + 1} \tag{3}$$

For brevity, a simplified symmetric form of the sigmoidal function is presented in Equation 3. This equation can be fitted to measured data to represent the relationship between Bruggeman effective medium fill factor and sample temperature. Further parameters can be added to the function to enable modelling of samples with an asymmetric transition. Here the parameters represent the transition temperature,T_c, and the width of the transition is set by P_1. Typical values to model the VO_2 transition are in the order of T_c = 340 and P_1 = 0.4.

Combining the biaxial effective medium (structural model) with the temperature-dependent VO_2 optical constants simulates the full optical response of the nanofin stack as it is heated through the IMT. Equilibrium emission in the normal direction is readily estimated from the normal incidence reflectance at each polarization and temperature weighted by the Planck blackbody spectrum. Predicted emission can be compared with the polarised emission measurements collected with the custom FTIR setup discussed next.

Method 3 - spectrally-resolved polarized emission measurements were carried out with a cus-

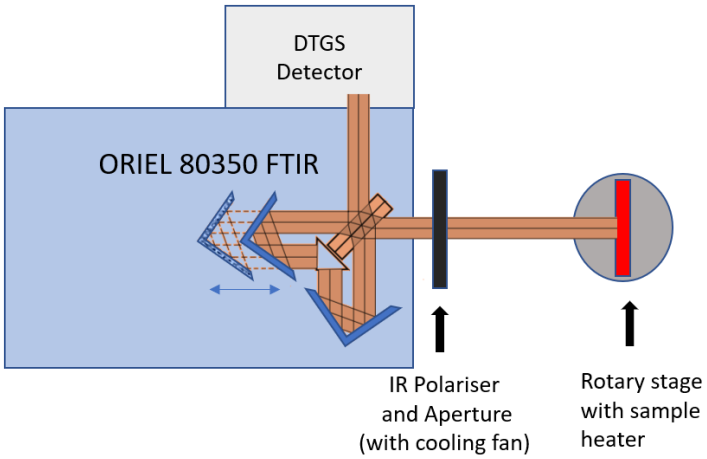

Fig 2 Schematic of FTIR setup for polarised emission measurements. The detector is an ambient-temperature dTGS.

tomized Oriel 80350 FTIR (Fourier transform infrared) spectrometer, in which the infrared source was replaced with a sample heater attached to a variable angle stage and rotating infrared wire-grid polarizer. Fig 2 displays a schematic of the customised FTIR setup utilised to take the direct emission measurements. We note that it is important to consider instrument configuration and calibration when measuring emittance.[26]

An ambient-temperature dTGS(triglycine sulfate) detector is utilised with a heated sample stage. Rather than controlling the stage temperature, the sample temperature is measured with a low thermal mass type-K thermocouple clamped on the front surface of the sample to minimise any variance in the temperature gradient throughout the sample/stage. The FTIR emission was calibrated using the measured temperature dependent emission from glass substrates with spectral properties established by reflection FTIR.

The background signal was minimised by the use of a large sample size of 75 mm x 50 mm and an aperture placed before the polarizer. Aperture and polarizer were kept near ambient by fan-forced convection. The use of a system with a room temperature dTGS detector, rather than a liquid nitrogen cooled mercury cadmium telluride (MCT) detector, dramatically simplifies calibration

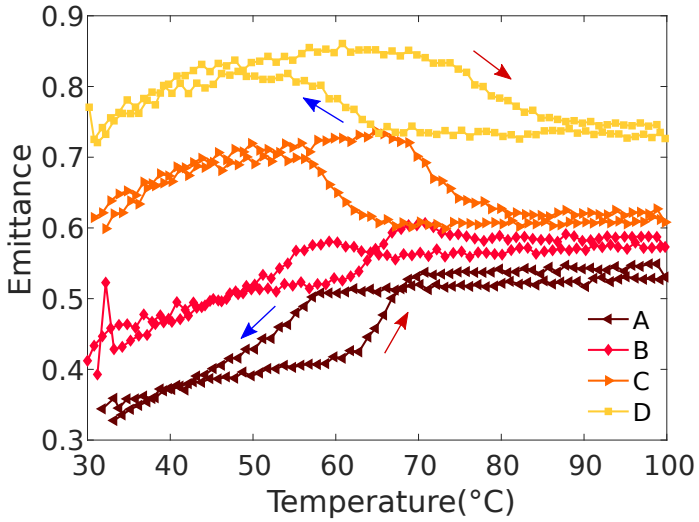

Fig 3 Integrated thermal emittance switching of VO_2 nano fins for increasing anneal times (A 4 hrs to D 11hrs) at 500°C in 0.2 Torr air. Red arrows indicate heating and blue are cooling.

because ambient temperature sources (such as optical components and reflections) produce zero signal. Since the heated sample acts as the source, emission measurements were performed at a minimum of 30 °C ($\sim$ 10 °C above ambient) to ensure sufficient signal. Temperature step times were chosen to ensure equilibrium was achieved. This system has been previously validated against reflection measurements across a wide range of temperatures with various temperature independent samples.

3 Results and Discussion

The switching of unpolarized spectrally-integrated emittance is an important first test in understanding the potential of these structures. We have discovered that the annealing time in air has a major effect on the emission switching profiles, with the final oxidized state having "regular" high-to-low emissivity switching. Fig. 3 shows the effect of temperature on the emittance of various samples annealed for differing times, with reverse switching only seen at shorter times. Here the unpolarised spectrally-integrated thermal emittance (Method 1) is used to measure each sample.

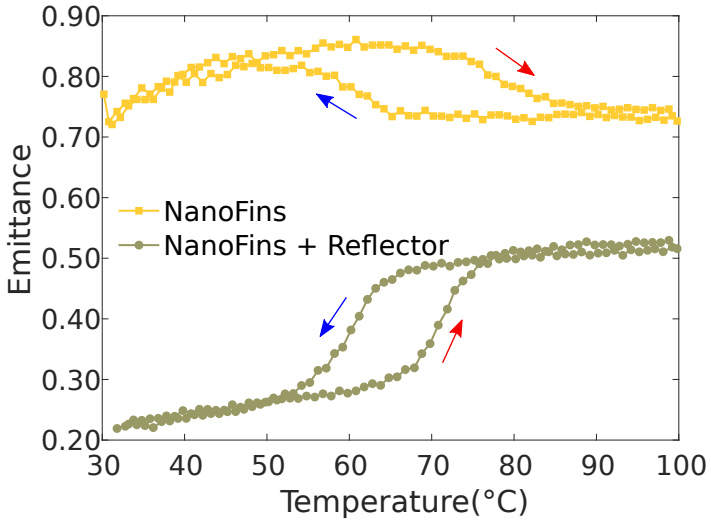

Fig 4 Integrated emittance switching of fully oxidized nano fins alone (yellow) and with an additional reflector(green). Both samples are annealed for 11hrs at 500°C in 0.2 Torr air. Red arrows indicate heating and blue are cooling

Since the fin production method typically leaves a solid underlayer, we propose that a nearly metallic V underlayer contributes to reverse switching at short oxidation times. To test this hypothesis, we added an additional 200nm thick V layer prior to deposition of the fins. As expected, the additional reflector reversed the switching direction for the longer anneal times (fully oxidized fins layer), as seen in Fig. 4. The magnitude of the emissivity changes are -0.13 and +0.30 for the fins alone and fins+reflector respectively, showing the potential from improved switching magnitude in addition to reversing the direction. In contrast, Fig.5 shows the how little the emittance of less-annealed samples is affected by an additional reflector. In both cases the emission switch is +0.25 which is somewhat less than the fully-oxidized fins with additional reflector. The negligible effect of the reflector on partially-oxidized fins is also consistent with the hypothesis that the underlayer is a major contributor to switching reversal, since those films retain a native metallic underlayer.

A fitted optical model is valuable for understanding and assessing the full potential of emission from these structures. Variable-angle polarized infrared reflection spectra, measured via Method 2, were fitted to a biaxial effective-medium model to estimate the nanofin structure and the underlayer

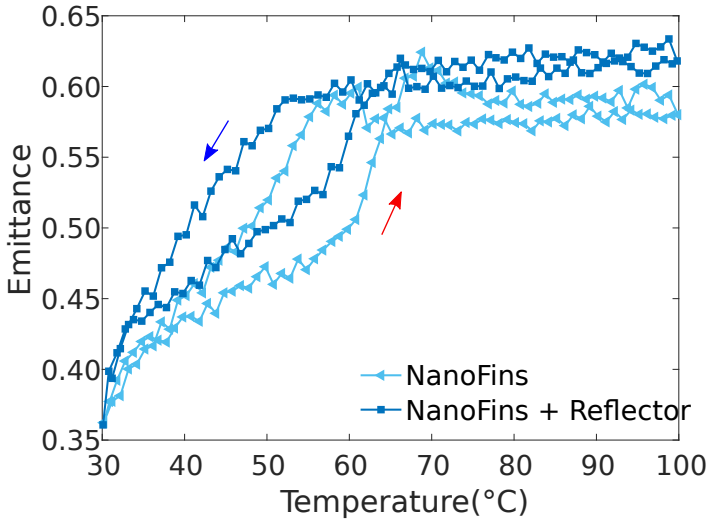

Fig 5 Integrated emittance of reverse switching fins (light blue), and with the addition of a 200nm vanadium base reflector (dark blue). Both were annealed for 4hrs. Red arrow indicate heating and blue is cooling.

Layer	Material	Short Anneal	Long Anneal
3	biaxial Bruggeman (VO_2/void)	0.80μm 53 % VO_2 depol ($L_{\parallel}$=0.29, $L_{\perp}$=0.71, L_{stack}=0.00)	0.61μm 20% VO_2 depol ($L_{\parallel}$=0.18, $L_{\perp}$=0.59, L_{stack}=0.23)
2	bulk VO_2	-	0.17μm
1	Vanadium	0.10μm	-
Substrate	Glass	1 mm	1mm

Table 1 Optical fit parameters of representative nanofin stacks with short and long anneal times.

thickness. The material optical properties used were that of solid thin films. Table 1 summarizes the parameter values determined for the 4 hr and 11 hr annealing times. Here Layer 3 represents the fin structure, with a biaxial Bruggeman effective medium approximation. The table includes the thickness, volume fraction of VO_2 and the biaxial depolarization factors which represent the shape of the fin structures.

Spectrally-resolved polarized emission measurements - Method 3, demonstrate the broad spectral range of these structures. Fig. 6 shows the normal emission radiance in temperature-wavelength space for parallel and perpendicular polarizations and their difference, comparing experimental emission measurements and with simulation based on the biaxial-Bruggeman model which was

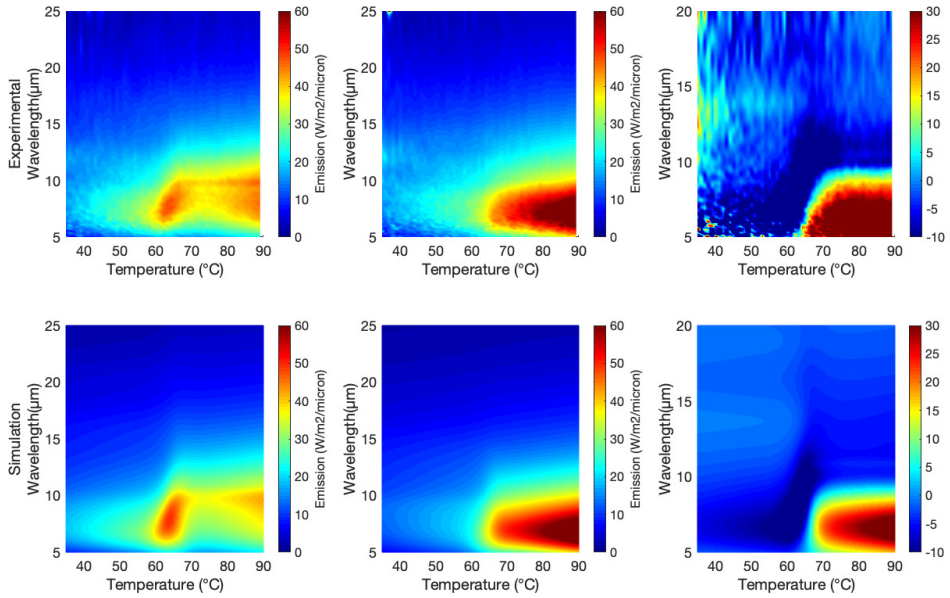

Fig 6 Polarized emission spectra as a function of temperature for a partially-oxidized nanofin stack, comparing measured experimental values (top row) and simulation model (bottom row). Left-most figures display the emission for the parallel polarization, middle figures indicate the perpendicular polarized emittance. Right figures display the polarization difference.

fitted to the infrared reflectance spectra. A large change in the emissions is observed in the 5-12 μm wavelength range, which is especially relevant to near-ambient thermal emission. In the parallel polarization a switch at $\sim$65 °C is also observed in the same wavelength range, although the change is smaller and at some wavelengths is reversed. Fig.6 displays the difference between the polarizations: the largest difference was observed for the hot state in the 5-10 μm wavelength range. The good match of the emissivity contours confirms the validity of the model used in the simulations.

The validated optical model for the nanofins can be used to assess the effect of various parameters and the maximum possible polarized emission switch. The calculated absorptance can be used to predict the temperature-induced (hot and cold state) change in the difference between normal-emittance for polarizations along and across the fins ($e_{H\parallel}$-$e_{H\perp}$)-($e_{C\parallel}$-$e_{C\perp}$), which we will

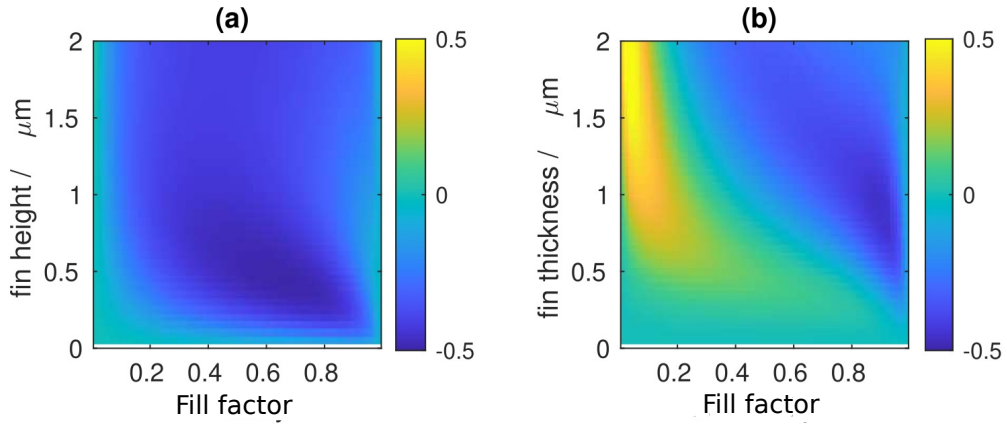

Fig 7 Maps of the "polarized emittance change" for depolarization ($L_{\|}$=0, $L_{\perp}$=1, L_{stack}=0) as a function of fin fill-factor and layer thickness, (a) without and (b) with reflector.

refer to as "polarized emittance change". This metric has a maximum magnitude of $\pm$ 2, and has been selected because it is unambiguously defined under spectral integration.

It is known that a biaxial Bruggeman model with extreme values of depolarization factors ($L_{\|}$ =0, $L_{\perp}$ =0) will usually have optimum in-plane polarization, so we can focus on the effect of the fill-factor (the amount of VO_2) and fin height, both with and without an underlying reflector. Fig. 7 demonstrates that, assuming sufficient height (e.g. $\sim$ 1 micron), the fill-factor of the fin layer has the most important effect on the polarization change. In the absence of an underlying reflector, the model predicts that heating will decrease the parallel polarization (-0.50 polarization change) at moderate fill-factors. With an underlying reflector, at low fill-factors the parallel polarization increases (+0.64 polarization change), whereas at high fill-factors the perpendicular polarization increases (-0.48 polarization change).

Further analysis reveals the details of the polarization response, summarized in Fig. 8. In the cold state (not shown), the fins are mostly unpolarized and transmitting, so the stack response is mostly unpolarized and determined by the underlayer (emitting or reflecting), whereas in the hot state the fin response also becomes important. The hot fins interact most strongly with the

parallel polarization: at low fill-factor they strongly emit (and moderately transmit) this polarization, whereas at moderate to high fill-factor they strongly reflect (and moderately emit) this polarization. The perpendicular polarization is mostly transmitted through the fins except at high fill-factor where the fins are moderately reflecting. If the underlayer is emitting, maximum polarization occurs at moderate a fill-factor, since parallel polarization is reflected and perpendicular is transmitted, leading to reduced parallel (and average) emittance. If the underlayer is reflecting, the hot stack emittance depends strongly on fin fill-factor. At low fill-factor, the hot fins emit some parallel polarization but do not couple to perpendicular, so the parallel (and average) emittance increases. Conversely at high fill-factor, the hot fins couple more to both polarizations but reflect mostly parallel, eventually resulting in a moderate increase of perpendicular emittance. The fitted experimental values of depolarization are not as extreme, with values (0, 0.29, 0.71) and (0.23, 0.18, 0.59) for the shortest and longest oxidation times respectively. However, Fig. 9 shows that if it were possible to optimize the fill-factor accordingly, the polarization change would be almost as strong as maximum depolarization. The samples used for developing the model with relatively shallow (0.6 to 0.8 μm) thickness and had relatively weak polarization change, e.g. sub-oxide with polarization change of only -0.04, and an oxide sample improved and reversed from -0.09 to +0.19 with the addition of a reflecting vanadium underlayer.

A thicker sample (black dot) had much stronger performance (-0.34). Although this thicker sample had a long oxidation, its visible backside reflectance, top-side color, spectral response and integrated performance were all consistent with VO_2 structure with a remnant non-oxidized reflecting vanadium underlayer. This highlights the importance of calibrating oxidation times to account for deposition parameters.

The VO_2 nano-structured films tested here showed no degradation during temperature-induced

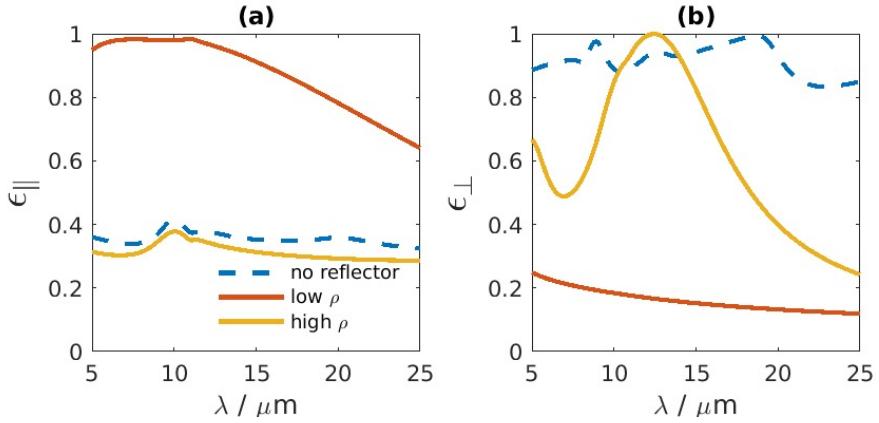

Fig 8 Predicted hot emittance spectra of optimal stacks, polarized (a) parallel and (b) perpendicular to the fins. Depolarization was ($L_{\parallel}$=0, $L_{\perp}$=1, L_{stack}=1). One result lacks a reflector (fin fill-factor 0.66 and height 0.45 microns), and the other two have a 1 micron V reflector(one with fin fill-factor 0.02 height 2.85 microns, and the other with fill-factor 0.90 and height 0.90 microns)

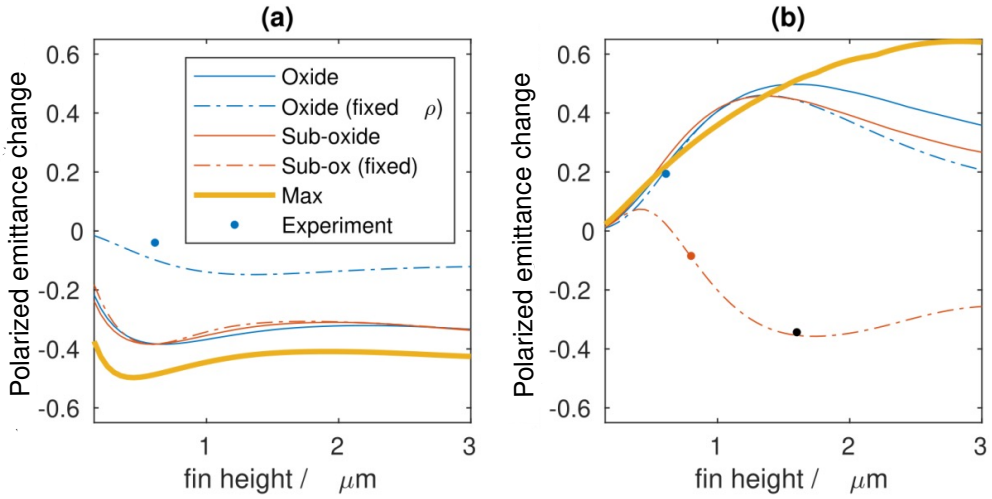

Fig 9 Predicted effect of fin layer height under various constraints, (a) without and (b) with reflector. ”Max” has extreme anisotropy and optimal fill-factor for a given height. ”Sub-oxide” corresponds to the shortest oxidation time, with optimal and experimental (fixed) fill-factor; “Oxide” corresponds to the longest oxidation time. Various experimental samples are shown as markers.

phase transition. Samples were cycled many times during differing testing runs and no change in response was observed. The samples were also observed to be shelf-stable and samples were still able to perform after many months of being stored in ambient conditions.

4 Conclusion

In summary the model clearly demonstrates the effect of the reflecting underlayer in reversing the polarization change, that polarization performance is sensitive to fill-factor (with changes occurring in either polarization), and that optimum performance can be achieved by fin layers around 1.5 micron thick. The annealing time is especially important because partial oxidation reverses the switching direction (due to unoxidized underlayer), and full oxidation restores the direction. Adding a metallic reflector to fully-oxidized fins also reverses the switch and produced a strong unpolarized emittance change (+0.30), at least doubling cooling power above the transition temperature. A biaxial effective medium stack provides an accurate model of the observed behavior and indicates a metallic underlayer when oxidation is incomplete. Direct emission measurements confirm a strong positive emission increase in the 5-12μm band for the polarization aligned with the fins for an incompletely oxidized layer. Optimization using the nanofin model predicts the importance of underlayer reflection, fin fill-factor and thickness, with a strong polarization change of 0.34 confirmed for sufficiently thick films.

Acknowledgments

C. E. and M. T. acknowledges support from the Australian Research Training Program. We thank Prof Michael Cortie for proofreading.

References

1 A. Tittl, A.-K. U. Michel, M. Schäferling, *et al.*, "A Switchable Mid-Infrared Plasmonic Perfect Absorber with Multispectral Thermal Imaging Capability," *Advanced Materials* **27**(31), 4597–4603 (2015).

2 Y. Qu, Q. Li, L. Cai, *et al.*, "Thermal camouflage based on the phase-changing material GST," *Light: Science & Applications* **7**(1), 26 (2018).

3 K.-K. Du, Q. Li, Y.-B. Lyu, *et al.*, "Control over emissivity of zero-static-power thermal emitters based on phase-changing material GST," *Light: Science & Applications* **6**(1), e16194–e16194 (2017).

4 E.-R. Sittner, K. S. Siegert, P. Jost, *et al.*, "(GeTe)x–(Sb2Te3)1–x phase-change thin films as potential thermoelectric materials," *physica status solidi (a)* **210**(1), 147–152 (2013).

5 F. J. Morin, "Oxides which show a metal-to-insulator transition at the neel temperature," *Physical Review Letters* **3**, 34–36 (1959).

6 Z. Yang, C. Ko, and S. Ramanathan, "Oxide Electronics Utilizing Ultrafast Metal-Insulator Transitions," *Annual Review of Materials Research* **41**, 337–367 (2011).

7 S. Taylor, Y. Yang, and L. Wang, "Vanadium dioxide based fabry-perot emitter for dynamic radiative cooling applications," *Journal of Quantitative Spectroscopy and Radiative Transfer* **197**, 76–83 (2017).

8 C. Lee, R. Atkins, W. Gibler, *et al.*, "Fiber optic application for thermal switching in vanadium dioxide films," *Applied optics* **28**(21), 4511–4512 (1989).

9 S. Chen, H. Ma, X. Yi, *et al.*, "Smart vo2 thin film for protection of sensitive infrared detectors from strong laser radiation," *Sensors and Actuators A: Physical* **115**(1), 28–31 (2004).

10 A. Hendaoui, N. Émond, S. Dorval, *et al.*, "Vo2-based smart coatings with improved emittance-switching properties for an energy-efficient near room-temperature thermal control of spacecrafts," *Solar Energy Materials and Solar Cells* **117**, 494–498 (2013).

11 E. Rephaeli, A. Raman, and S. Fan, "Ultrabroadband photonic structures to achieve high-performance daytime radiative cooling," *Nano Letters* **13**, 1457–1461 (2013).

12 S.-H. Wu, M. Chen, M. T. Barako, *et al.*, "Thermal homeostasis using microstructured phase-change materials," *Optica* **4** (2017).

13 M. Ono, K. Chen, W. Li, *et al.*, "Self-adaptive radiative cooling based on phase change materials," *Opt. Express* **26**, A777—-A787 (2018).

14 M. A. Kats, R. Blanchard, S. Zhang, *et al.*, "Vanadium dioxide as a natural disordered metamaterial: Perfect thermal emission and large broadband negative differential thermal emittance," *Phys. Rev. X* **3**, 041004 (2013).

15 Choi, Ahn, Jung, *et al.*, "Mid-infrared properties of a vo2 film near the metal-insulator transition.," *Physical review. B, Condensed matter* **54 7**, 4621–4628 (1996).

16 A. R. Gentle, G. B. Smith, and A. I. Maaroof, "Frequency and percolation dependence of the observed phase transition in nanostructured and doped VO2 thin films," *Journal of Nanophotonics* **3**(1), 1–15 (2009).

17 X. Wang, Y. Cao, Y. Zhang, *et al.*, "Fabrication of VO 2 -based multilayer structure with variable emittance," *Applied Surface Science* **344**, 230–235 (2015).

18 A. Hendaoui, N. Émond, M. Chaker, *et al.*, "Highly tunable-emittance radiator based on semiconductor-metal transition of VO2 thin films," *Applied Physics Letters* **102** (2013).

19 K. Sun, C. A. Riedel, A. Urbani, *et al.*, "VO2 Thermochromic Metamaterial-Based Smart Optical Solar Reflector," *ACS Photonics* **5**, 2280–2286 (2018).

20 K. Ito, T. Watari, K. Nishikawa, *et al.*, "Inverting the thermal radiative contrast of vanadium dioxide by metasurfaces based on localized gap-plasmons," *APL Photonics* **3**, 86101 (2018).

21 A. R. Gentle, M. C. Tai, S. White, *et al.*, "Design, control, and characterisation of switchable radiative cooling," in *New Concepts in Solar and Thermal Radiation Conversion and Reliability*, J. N. Munday, P. Bermel, and M. D. Kempe, Eds., **10759**, 16, SPIE (2018).

22 M. C. Tai, A. R. Gentle, M. D. Arnold, *et al.*, "Spontaneous growth of polarizing refractory metal 'nano-fins'," *Nanotechnology* **29**, 105702 (2018).

23 Y. Qu, Q. Li, L. Cai, *et al.*, "Polarization switching of thermal emissions based on plasmonic structures incorporating phase-changing material Ge2Sb2Te5," *Optical Materials Express* **8**(8), 2312–2320 (2018).

24 D. E. Aspnes, J. B. Theeten, and F. Hottier, "Investigation of effective-medium models of microscopic surface roughness by spectroscopic ellipsometry," *Phys. Rev. B* **20**, 3292–3302 (1979).

25 D. A. G. Bruggeman, "Berechnung verschiedener physikalischer Konstanten von heterogenen Substanzen. I. Dielektrizitätskonstanten und Leitfähigkeiten der Mischkörper aus isotropen Substanzen," *Annalen der Physik* **416**(7), 636–664 (1935).

26 Y. Xiao, C. Wan, A. Shahsafi, *et al.*, "Precision Measurements of Temperature-Dependent and Nonequilibrium Thermal Emitters," *Laser & Photonics Reviews* **14**(8), 1900443 (2020).

Caleb Estherby is a third year PhD student in applied physics studying at the University of Technology Sydney. He received his BSc(Honours) in applied physics with first class honours in 2019.

Working under Dr Angus Gentle and A/Prof. Matthew D. Arnold on the working title ”Dynamically Re-configurable Optical Surfaces”. His current research interests include re-configurable surfaces, spectrally selective coatings, optical computing, optical characterisations and vanadium dioxide applications.

Matthew Arnold is an Associate Professor at the University of Technology Sydney. He received his BSc(Hons) and PhD degrees in physics from the University of Otago in 2000 and 2005 respectively. He is the author of more than 70 scientific publications. His current research interests include emergent phenomena, optical nanostructures, polarizing materials and plasmonics. He is a Senior Member of SPIE.

Matthew Tai is a consultant with Pipeline Condition Assessment (PCA), a division of ADE Consulting Group. He received his BSc(Nanotechnology), BSc(Hons),and PhD degree in Physics from UTS in 2013, 2014 and 2019, respectively.

Angus Gentle is a Lecturer at the University of Technology, Sydney (UTS). He received his BSc(Applied Physics), BE(Electrical) and PhD degree in physics from UTS in 2003, 2005 and 2008, respectively. He is the author of more than 90 journal and conference papers. His current research interests include radiative cooling, re-configurable surfaces, spectrally selective coatings.

List of Figures

List of Tables